Published paper

Huyanan, S. and Sims, N.D. Vibration Control Strategies for Proof-mass Actuators. *Journal of Vibration and Control*, 2007, **13**(12), 1785-1806.

http://dx.doi.org/10.1177/1077546307080031

Vibration control strategies for proof-mass actuators

Satienpong Huyanan and Neil D Sims[1]

Advanced Manufacturing Research Centre with Boeing,

Department of Mechanical Engineering,

The University of Sheffield

Mappin St, Sheffield S1 3JD, UK

Abstract

Proof-mass actuators have been considered for a broad range of structural vibration control problems, from the seismic protection of tall buildings, to the improvement of metal machining productivity by increasing the stability of self-excited vibrations known as chatter. In general this broad range of potential applications means that a variety of controllers have been proposed, without drawing direct comparisons with other controller designs that have been considered for different applications.

This article takes three controllers that are potentially suitable for the machining chatter problem: direct velocity feedback, tuned-mass-damper control (or vibration absorber control), and active-tuned-mass-damper control (or active vibration absorber control). These control strategies are restated within the more general framework of Virtual Passive Control. Their performance is first compared using root locus techniques, with a model based upon experimental data that includes the low frequency dynamics of the proof mass. The frequency response of the test structure is then illustrated under open and closed-loop conditions. The application of the control strategies to avoid machine-tool chatter vibrations is then discussed, without going into detail on the underlying physical mechanisms of chatter. It is concluded that virtual passive absorber control is more straightforward to implement than virtual skyhook damping, and may be better suited to the problem of machining chatter.

Keywords: proof mass actuator; active vibration control; machine tool chatter; virtual passive control.

---

[1] Corresponding author. Email: n.sims@sheffield.ac.uk. Tel: +44 114 2227724. Fax: +44 114 2227890.

Introduction

In the past decades, active vibration control methods have received widespread attention for applications varying from civil structures (Guclu and Sertbas (2005; Nishimura et al. (1992; Nishimura et al. (1998)) to milling machines (Chung et al. (1997)) and space satellites (Hagood and Crawley (1991)). One popular means of achieving active vibration control is through the use of proof-mass actuators (Preumont (2002)), which comprise a mass supported on a compliant suspension. A reaction force on the host structure is produced by the inertia of the mass to the excited electromagnet force. Perhaps the most straightforward control strategy implemented on this device is direct velocity feedback (Preumont (2002)). As the name suggests, the damping of the host structure is increased by inducing a control force proportional to the absolute velocity of the structure at the location of the actuator. The control strategy can therefore be considered as a virtual skyhook damper. Along similar lines, the actuator can be made to behave as any configuration of 'virtual' passive devices, using the philosophy of virtual passive control described by Juang and Phan (2001). Alternatively, fully active control laws can be developed based upon the principles of classical (Guclu and Sertbas (2005)), sliding mode (Cao et al. (2000)), or optimal (Wang and Cheng (1989)) control methods.

The objective of the present study is to compare the performance of a selection of controller designs using an experimental and numerical approach. The intended application of the vibration control system is the suppression of undesirable chatter vibrations during milling of a flexible workpiece. Similar solutions have been developed for milling machine structures by Chung et al. (1997) and for other machining applications by Pratt and Nayfeh (2001), but the problem of milling workpiece chatter remains open.

For this specific application, it is desirable to implement a controller that is relatively straightforward to design and tune, and at the same time offers some robustness to changes in dynamics of the host structure. These changes in dynamics are inevitable as material is removed from the workpiece during machining. For these reasons, the present study will compare the performance of three control strategies: Virtual skyhook control, virtual passive absorber control, and a hybrid virtual passive/active vibration absorber control strategy.

The virtual skyhook strategy was chosen because it has been successfully implemented on machine structures (not workpieces) for chatter mitigation by Chung et al. (1997) and Ganguli et al. (2005). Virtual vibration absorbers have been considered for chatter avoidance in turning by Pratt and Nayfeh (2001). They may offer superior performance than the skyhook approach, but to date it appears that no work has been done to directly compare performance for chatter avoidance applications.

It should be pointed out at this stage that the control strategies will be benchmarked without the added complexity of implementing active control during machining. Instead, the paper focuses on a laboratory based vibration study and interprets the results from the perspective of chatter vibrations. Where necessary the background theory of chatter is briefly mentioned rather than resorting to a detailed description which can be found elsewhere, such as Tlusty (2000).

The paper is organised as follows. To begin, the theoretical basis of the control strategies used in this study is described. The experimental study is then introduced, and models of the structure and actuator are developed. Root locus techniques are then used to illustrate the behaviour of the three control strategies. Experimental and simulated results are presented, and the closed-loop behaviour is discussed. Finally, some conclusions are drawn.

Theory

The background theory regarding proof-mass actuators, and the three control strategies, will now be introduced. Although much of this information could be obtained from the existing literature, a detailed description serves as a useful tutorial exercise. Furthermore, this opportunity will be used to restate the control strategies within the more general framework known as virtual passive control.

Proof mass actuators

A proof-mass actuator system is comprised of a reaction mass m_p supported on a spring k_p and damper c_p attached to the base as illustrated in Figure 1. The reaction mass is excited by an electromagnetic force f_c according to the voltage input V_{in}. The transfer function between the proof-mass displacement x_p and the voltage input V_{in} can be written as,

$$\frac{x_p(s)}{V_{in}(s)} = \frac{G_1 G_2}{m_p s^2 + c_p s + k_p} \tag{1}$$

where G_1 is the electromagnetic gain and G_2 is the power amplifier gain (Preumont (2002)).

The reaction force f_a on the supporting base is a product of the actuator's mass and acceleration. This yields the transfer function between the reaction force f_a and the voltage input V_{in}:

$$\frac{f_a(s)}{V_{in}(s)} = \frac{-G_1 G_2 m_p s^2}{m_p s^2 + c_p s + k_p} = g_a \frac{s^2}{s^2 + 2\zeta_p \omega_p s + \omega_p^2} \tag{2}$$

where ω_p is the natural frequency, ζ_p is the damping ratio of the proof-mass actuator and g_a is the actuator gain.

Figure 2 illustrates the bode plots of an ideal proof-mass actuator, which behaves as a zeroth-order force generator beyond the operating frequency ω_c. The proof-mass natural frequency ω_p can be adjusted by changing the mass m_p, whilst the critical frequency ω_c is the lower frequency limit of the proof-mass operating range. In practice, this suggests that the actuator can be used to effectively control vibrations at frequencies above ω_c and below the bandwidth of the electromagnetic circuit. Within this region, the device can be thought of as an active force generator, which can control structural vibrations as shown in Figure 3a. However, a suitable control strategy is required to determine the actuation force F_a.

Virtual skyhook damping

In a skyhook damper with acceleration feedback, the control law from the acceleration output $s^2X(s)$ to the voltage command $V_c(s)$ can be written as:

$$V_c(s) = -\frac{g_i}{s} \cdot s^2 X(s) \tag{3}$$

where g_i is the integral controller gain.

Considering an ideal force actuator with the actuator gain g_a, the actuator transfer function between the force output $F_a(s)$ and the voltage input $V_c(s)$ is simply,

$$F_a(s) = g_a \cdot V_c(s) \tag{4}$$

Substituting Equation (2) into Equation (1) yields the active control law:

$$F_a(s) = -g_{sky} \cdot \frac{1}{s} \cdot s^2 X(s) = -g_{sky} \cdot sX(s) \tag{5}$$

where $g_{sky} = g_a \cdot g_i$. Since the active control force is proportional to the structure velocity, the controller is also referred to as Direct Velocity Feedback. The strategy is illustrated schematically in Figure 3(b). Considering a single-input/single-output (SISO) system

described by a transfer function $G(s)$, the corresponding closed-loop characteristic equation of the system with the Virtual Skyhook Damping (VSD) controller is simply,

$$1 + g_{sky} \cdot s \cdot G(s) = 0 \tag{6}$$

If the active damping force is produced by a proof mass actuator, the system closed-loop characteristic equation with the actuator dynamics can be written as,

$$1 + g_{sky} s \frac{s^2}{s^2 + 2\zeta_p \omega_p s + \omega_p^2} \cdot G(s) = 0 \tag{7}$$

which can be used to explore the influence of the proof-mass dynamics on the controller performance.

This is perhaps the most straightforward example of a virtual passive controller for a proof mass actuator. At this stage, it is worth describing the general principles of virtual passive control in a little detail, before going on to describe the specific case of virtual vibration absorbers.

Virtual passive control

The dynamics of any linear mechanical system can be represented by two sets of second order ordinary differential equations in the time domain, in the form (Juang and Phan (2001)):

$$\underline{M}\ddot{x} + \underline{C}\dot{x} + \underline{K}x = F_d + \underline{B}u \tag{8}$$

$$y = \underline{H}_a\ddot{x} + \underline{H}_v\dot{x} + \underline{H}_d x \tag{9}$$

where x is an $n \times 1$ displacement vector; $\underline{M}$, $\underline{C}$ and $\underline{K}$ are the $n \times n$ matrices of mass, damping and stiffness, respectively; $\underline{B}$ is the $n \times r$ influence matrix of the $r \times 1$ actuator force distributions vector u and F_d is the $n \times 1$ disturbance forces vector externally excited the system. equation (9) represents a measurement equation of the $m \times 1$ measurement vector and $\underline{H}_a$, $\underline{H}_v$ and $\underline{H}_d$ are $m \times n$ influence matrices of acceleration, velocity and displacement

respectively. The measurement vector y can be used either directly as direct state feedback or indirectly as input to a controller.

Consider a controller with second-order dynamics which is modelled in the form

$$\underline{M}_c\ddot{x}_c + \underline{C}_c\dot{x}_c + \underline{K}_c x_c = \underline{B}_c u_c \tag{10}$$

The equivalent measurement equation of the controller is defined by

$$y_c = \underline{H}_{ac}\ddot{x}_c + \underline{H}_{vc}\dot{x}_c + \underline{H}_{dc}x_c \tag{11}$$

Equation (10) represents a fictitious controller model, where x_c is an $n_c \times 1$ controller displacement vector. $\underline{M}_c$, $\underline{C}_c$ and $\underline{K}_c$ represented virtual mass, damping and stiffness matrices of the controller; $\underline{B}_c$ is the $n_c \times m$ influence matrix of the $m \times 1$ input force vector u_c. The $r \times 1$ controller output vector y_c is described by the virtual measurement equation (11) where $\underline{H}_{ac}$, $\underline{H}_{vc}$ and $\underline{H}_{dc}$ are the $r \times n_c$ influence matrices of the controller acceleration, velocity and displacement, respectively. The closed-loop control system is then accomplished by coupling the system to the controller, this yields:

$$u = y_c = \underline{H}_{ac}\ddot{x}_c + \underline{H}_{vc}\dot{x}_c + \underline{H}_{dc}x_c \tag{12}$$

$$u_c = y = \underline{H}_a\ddot{x} + \underline{H}_v\dot{x} + \underline{H}_d x \tag{13}$$

Substituting equations (12) and (13) into equations (8) and (10) yields the closed-loop system equation:

$$\underline{M}_t\ddot{x}_t + \underline{C}_t\dot{x}_t + \underline{K}_t x_t = F_t \tag{14}$$

where

$$\underline{M}_t = \begin{bmatrix} \underline{M} & -\underline{B}\underline{H}_{ac} \\ -\underline{B}_c\underline{H}_a & \underline{M}_c \end{bmatrix},\ \underline{C}_t = \begin{bmatrix} \underline{C} & -\underline{B}\underline{H}_{vc} \\ -\underline{B}_c\underline{H}_v & \underline{C}_c \end{bmatrix}$$

$$\underline{K}_t = \begin{bmatrix} \underline{K} & -\underline{B}\underline{H}_{dc} \\ -\underline{B}_c\underline{H}_d & \underline{K}_c \end{bmatrix},\ F_t = \begin{bmatrix} F_d \\ 0 \end{bmatrix} \text{ and } x_t = \begin{bmatrix} x \\ x_c \end{bmatrix}$$

The controller must be designed by choosing the quantities $\underline{M}_c$, $\underline{C}_c$, $\underline{K}_c$, $\underline{H}_{ac}$, $\underline{H}_{vc}$ and $\underline{H}_{dc}$ such that $\underline{M}_t$ becomes positive definite whereas $\underline{C}_t$ and $\underline{K}_t$ become positive definite or positive semi-definite to ensure an asymptotically stable system. The following sections discuss the special cases where virtual passive absorber dynamics and virtual passive/active absorber dynamics are desired.

Virtual Passive Absorber (VPA) controller

Consider a SDOF passive vibration absorber attached to the structure as shown in Figure 3(c). The equations of motion of the system can be written as,

$$M\ddot{x} + C\dot{x} + Kx = F_d - c_a\dot{z} - k_a z \tag{15}$$

$$m_a\ddot{z} + c_a\dot{z} + k_a z = m_a\ddot{x} \tag{16}$$

Here, z defines the absorber relative displacement; m_a, c_a and k_a are mass, damping and stiffness of the absorber. The virtual passive controller can be designed to represent the passive vibration absorber given in equation (15) by simply letting $x_c = z$ such that $\underline{M}_c = \underline{B}_c = m_a$, $\underline{C}_c = c_a$ and $K_c = k_a$. Using acceleration feedback with a collocated sensor-actuator, this gives $u_c = y = \ddot{x}$ and $y_c = u$. Now, the measurement equation (9) has only acceleration measurement, thus giving that $H_a = 1$ and $H_v = H_d = 0$. By introducing $\underline{B} = 1$ into equation (8), the actuation input u to the system becomes,

$$u = y_c = -c_a\dot{z} - k_a z \tag{17}$$

Equating the coefficients of equation (17) to the controller measurement equation (11), gives $\underline{H}_{ac} = 0$, $\underline{H}_{vc} = -c_a$ and $\underline{H}_{dc} = k_a$. The system with a virtually attached passive absorber is illustrated in Figure 3(d), and the virtual passive absorber (VPA) control law with acceleration feedback can be stated as,

$$m_a\ddot{x}_c + c_a\dot{x}_c c + k_a x_c = m_a y \tag{18}$$

$$u = y_c = -c_a\dot{x}_c - k_a x_c \tag{19}$$

where $y = \ddot{x}$ is the acceleration of the primary structure, which can be directly acquired using an accelerometer. This indicates that the control law is readily implemented in practice. Furthermore, the VPA can be simplified by representing in dimensionless form as,

$$\ddot{x}_c + 2\zeta_c\omega_c\dot{x}_c + \omega_c^2 x_c = \ddot{x} \tag{20}$$

$$u = y_c = M\mu_c\left(-2\zeta_c\omega_c\dot{x}_c - \omega_c^2 x_c\right) \tag{21}$$

where ω_c and ζ_c are natural frequency and damping ratio of the controller, and μ_c defines a ratio of the controller mass m_c to the system mass M. The state equation of the controller can be written as,

$$\left.\begin{aligned} \begin{bmatrix}\dot{x}_c \\ \ddot{x}_c\end{bmatrix} &= \begin{bmatrix}0 & 1 \\ -\omega_c^2 & -2\zeta_c\omega_c\end{bmatrix}\cdot\begin{bmatrix}x_c \\ \dot{x}_c\end{bmatrix} + \begin{bmatrix}0 \\ 1\end{bmatrix}\cdot y \\ u = y_c &= M\mu_c\begin{bmatrix}-\omega_c^2 & -2\zeta_c\omega_c\end{bmatrix}\cdot\begin{bmatrix}x_c \\ \dot{x}_c\end{bmatrix} + [0]\cdot y \end{aligned}\right\} \tag{22}$$

The optimal VPA controller parameters can be determined based on the methods used to optimize a passive absorber, which can be directly determined from the structural modal parameters. The natural frequency and damping ratio of the virtual absorber can be optimized in the same way as for a passive damped absorber attached to an undamped primary structure. Rather than repeat the analysis given by Den Hartog (1985), Ormondroyd (1928), and Juang (1992, 2001), the optimal passive absorber parameters are listed in Table 1.

This optimisation requires knowledge of the modal parameters of the host structure. If these parameters are not known accurately, a passive absorber will still be stable, but may not yield a desirable performance. In contrast, a *virtual* passive absorber that is realised with a proof mass actuator may become unstable due to the low-frequency dynamics of the actuator. This issue can be investigated by considering the characteristic equation of the system.

Let $G(s)$ describe a transfer function of a SISO system. The corresponding closed-loop characteristic equation of the system with the VPA controller including the proof-mass dynamics can then be described as,

$$1+\frac{g_a s^2}{\left(s^2+2\zeta_p\omega_p s+\omega_p^2\right)}\cdot\frac{M\mu_c s^2\left(2\zeta_a\omega_a s+\omega_a^2\right)}{g_a\left(s^2+2\zeta_a\omega_a s+\omega_a^2\right)}\cdot G(s)=0 \tag{23}$$

Here, $1/g_a$ is multiplied to compensate for the actuator gain. Equation (23) will be used later on to investigate the stability of the experimental system.

Virtual passive/active absorber (VPAA)

The VPA controller can be extended to include an active control law. The idea is to implement a passive/active control law using an Active Tuned Mass Damper (ATMD) with acceleration feedback, as presented by Nishimura *et al* (1992). In their study, a passive tuned mass device was supplemented with a force actuator, leading to the equations of motion of a single-degree-of-freedom system with ATMD device as,

$$M\ddot{x}+C\dot{x}+Kx=F_d-c_a\dot{z}-k_a z+f_u(t) \tag{24}$$

$$m_a\ddot{z}+c_a\dot{z}+k_a z=m_a\ddot{x}+f_u(t) \tag{25}$$

$$f_u(t)=Mg_u\ddot{x} \tag{26}$$

where g_u is the direct acceleration feedback gain which is a ratio to the system mass M. From equation (25), the coupling force between the ATMD to the structure can be stated as:

$$F_{coupling}=-c_a\dot{z}-k_a z+Mg_u\ddot{x}=-m_a\left(\ddot{x}-\ddot{z}\right) \tag{27}$$

In the present study, the same active control law will be used but the passive absorber will be implemented 'virtually' (i.e. by the controller) rather than physically (i.e. with a spring-mass-damper arrangement), as shown in Figure 3(e). Compared to the virtual passive absorber (Figure 3(d)) the control law now allows energy to be injected into the host structure, as well

as dissipated. Upon substitution of equations (24), (25) and (26) into the virtual controller (equations (10) and (11)), this yields the matrices $\underline{M}_t$, $\underline{C}_t$ and $\underline{K}_t$:

$$\underline{M}_t = \begin{bmatrix} M - Mg_u & 0 \\ -m_c + Mg_u & m_c \end{bmatrix}, \underline{C}_t = \begin{bmatrix} C & -c_c \\ 0 & c_c \end{bmatrix} \text{ and } \underline{K}_t = \begin{bmatrix} K & -k_c \\ 0 & k_c \end{bmatrix}$$

Here, $\underline{C}_t$ and $\underline{K}_t$ are positive definite, and the system is stable only if $\underline{M}_t$ becomes positive definite for $g_u < 1$. Considering a system with an acceleration feedback with collocated sensor/actuator, this yields $\underline{H}_a = \underline{B} = \underline{H}_a = 1$ and $\underline{H}_v = \underline{H}_d = 0$. Meanwhile equation (9), $y = u_c = \ddot{x}$ and $\underline{B}_c = \left(m_a - Mg_u\right)$. Thus, the virtual passive/active vibration absorber controller can be stated as

$$m_c\ddot{x}_c + c_c\dot{x}_c + k_c x_c = \left(m_a + Mg_u\right)\ddot{x} \tag{28}$$

$$u = -c_c\dot{z} - k_c z + Mg_u\ddot{x} \tag{29}$$

The controller parameters can be represented in dimensionless form as:

$$\ddot{x}_c + 2\zeta_c\omega_c\dot{x}_c + \omega_c^2 x_c = \left(1 + {g_u}/{\mu}\right)\ddot{x} \tag{30}$$

$$u = M\mu_c\left(-2\zeta_c\omega_c\dot{z} - \omega_c^2 z + {g_u}/{\mu_c}\ \ddot{x}\right) \tag{31}$$

where ω_c and ζ_c are the natural frequency and damping ratio of the controller, $\mu_c = m_c/M$ and $g_u < 1$, respectively. The controller state equation can be written as:

$$\left.\begin{aligned} \begin{bmatrix} \dot{x}_c \\ \ddot{x}_c \end{bmatrix} &= \begin{bmatrix} 0 & 1 \\ -\omega_c^2 & -2\zeta_c\omega_c \end{bmatrix} \cdot \begin{bmatrix} x_c \\ \dot{x}_c \end{bmatrix} + \begin{bmatrix} 0 \\ 1 + {g_u}/{\mu_c} \end{bmatrix} \cdot y \\ u = y_c &= M\mu_c\left(\begin{bmatrix} -\omega_c^2 & -2\zeta_c\omega_c \end{bmatrix} \cdot \begin{bmatrix} x_c \\ \dot{x}_c \end{bmatrix} + \begin{bmatrix} {g_u}/{\mu_c} \end{bmatrix} \cdot y\right) \end{aligned}\right\} \tag{32}$$

where $y = \ddot{x}$ is an acceleration of the primary structure directly acquired from an accelerometer. All that remains is to choose optimal values for the controller parameters, which were analytically derived by Nishimura *et al* (1992) based on a frequency domain equal-peak method. The resulting optimum parameters resemble those for passive Den Hartog

(1985) optimisation, except for the addition of the active gain g_u. The optimum natural frequency and damping ratio of the ATMD controller are listed in Table 1.

Again, the low-frequency dynamics of the proof mass may influence the stability of the control system so it is useful to consider the characteristic equation of the system. For a SISO system described by a transfer function $G(s)$, the corresponding characteristic equation of the closed-loop system including the actuator dynamics can be written as,

$$1+\frac{g_a s^2}{\left(s^2+2\zeta_p\omega_p s+\omega_p^2\right)}\cdot\frac{M}{g_a}\left[\frac{\mu_c\left(1+g_u/\mu_c\right)s^2\left(2\zeta_a\omega_a s+\omega_a^2\right)}{\left(s^2+2\zeta_a\omega_a s+\omega_a^2\right)}-g_u s^2\right]\cdot G(s)=0 \qquad (33)$$

where, $1/g_a$ is multiplied to compensate the actuator gain.

To summarise, the three control strategies are presented schematically in Figure 3, and their characteristic equations are given in equations (7), (23), and (33). The next section will introduce an experiment that will be used to investigate the performance of these control strategies. Models of the experimental system will also be developed, so that the characteristic equations can be solved and compared under different controller gains.

Experimental method

Experimental setup

This study is concerned with controlling vibration of the aluminium 'workpiece' structure, and the experimental setup is shown in Figure 4. The aluminium workpiece is mounted rigidly to the base, and an electromagnetic shaker (LDS-V406) was used to excite the structure. A co-located force sensor (1) and accelerometer (2) were used to measure the structure's response, and its frequency responses were then processed using SigLab data acquisition hardware (6). The active control system is a SISO system implemented on a collocated proof mass actuator (4) and accelerometer (3) according to the control voltage fed

from the controller. The proof mass actuator was constructed from a commercial PC speaker-amplifier system using its weight as a proof mass, and a long cable was used to suspend the proof-mass. The actuator was attached to the structure by an extension rod at a selected control site, as shown in Figure 5. The controllers were implemented using the xPC target real time control system (5), running in a Matlab environment.

Identification of the structure and actuator

The modal parameters of the test structure were first identified by performing frequency response testing under open-loop conditions. The structure was excited at coordinate X_1, and acceleration responses were observed at coordinate X_1, X_2 and X_3, as illustrated in Figure 4. The structural frequency responses were then processed using the Siglab system. The peak-amplitude method (Ewins (2000)) was used to extract modal parameters of the structure, and the extracted modal parameters are shown in Table 2. Since the first two modes were the control target in this study, a reduced-order model of the structure was then developed. A typical frequency response of the reduced model is compared with the experimental results in Figure 6(a). The transfer function of the structure at coordinate X_1 and X_2 to the excitation force F_d can be stated as,

$$\begin{bmatrix} X_1 \\ X_2 \end{bmatrix} = \begin{bmatrix} \dfrac{1.961\ s^2 + 247.6\ s + 6.736\text{e}007}{s^4 + 211.2\ s^3 + 5.914\text{e}007\ s^2 + 1.994\text{e}009\ s + 3.822\text{e}014} \\ \dfrac{1.192}{s^2 + 9.783\ s + 7.385\text{e}006} \end{bmatrix} F_d(s) \qquad (34)$$

In performing a frequency response test to characterise the actuator, the speaker was mounted in horizontal position to a large rigid base. A chirp harmonic signal was used to drive the actuator, and an accelerometer was used to measure the proof mass response. The proof mass transfer function was then processed with SigLab, and the actuator mass m_p (0.12kg) was multiplied to obtain the output force per unit input voltage. Figure 6(b) shows the FRF of the proof mass actuator. The actuator exhibits almost ideal force generator characteristics within

the frequency range 350Hz to 2000Hz. Based on the modal parameters extracted, the force output $f_a(s)$ to voltage input $V_m(s)$ transfer function of the proof mass actuator can be written as,

$$\frac{f_a(s)}{V_{in}(s)} = -1.32 \times \frac{s^2}{s^2 + 410.5s + 3.8693 \times 10^5} \tag{35}$$

This model agrees well with the experimental result as shown by Figure 6(b). The high frequency characteristics were ignored to simplify this study. However complex mode dynamics of the actuator were visible at frequencies higher than 1600Hz.

Controller implementation

The controllers were implemented using the xPC target system, which relies on a Simulink model (shown in Figure 7), that is developed on the host PC. The xPC target application is then created and downloaded to the target PC. A multi-channel IO-card (NI PCI-MIO-16E-4) was used to interface to the controller from the accelerometer and proof mass actuator, with a sampling period of 50μs. The controller block represents the control law described by either equations (5), (22) or (32) (depending on the controller implemented). The compensator block represents an additional modification to two of the controllers: a low-pass filter in the VSD controller and a high-pass filter in the VPAA controller. For the VSD controller, the accelerometer signal was found to drift excessively, and so the compensator was introduced to filter out this low frequency deviation. Meanwhile, the VPAA controller was sensitive to high frequency noise and vibration, so the compensator was a low-pass filter. In contrast, the VPA controller did not need any compensation and so a unity gain (pass-through) was used for the compensator.

All that remains is to choose appropriate values for the controller gains, for each of the control strategies under consideration. For the vibration absorber based designs, tuning parameters can be determined using the formulae in Table 1. However, it is useful to compare

the performance of all the controllers using root locus techniques, based upon the 2DOF model of the structure (equation (34)).

Root locus analysis

For the virtual skyhook control strategy, the root locus is shown in Figure 8. Here, the structure is modelled as a 2-DOF system and the controller gain g_{sky} is increased to develop the root locus. The proof-mass dynamics are neglected in Figure 8(a), whilst they are included in Figure 8(b). The system in Figure 8(a) possesses alternating poles and zeros, indicating that the root locus will always lie to the left of the poles and zeros. Consequently the system stability is guaranteed for this model. In contrast, the inclusion of the low-frequency dynamics of the actuator (Figure 8(b)) has disrupted the sequence of alternating poles and zeros. Stability is no longer guaranteed for this model, which becomes unstable as the gain g_{sky} increases. Consequently, either the actuator must be designed with a high damping ratio or a cascade compensator must be implemented to place the complex pole pair further away from the imaginary axis. In this study, the controller gain was chosen to be g_{sky}=300 to achieve a stable response.

For the virtual passive absorber, optimum parameters can be determined (for a given mass ratio μ_c) using Table 1. This results in changing open-loop poles and zeros of the system as the gain μ_c increases, and so a classical root locus plot is not strictly applicable. However, the stability of the system can still be observed from the location of its characteristic roots. The loci of characteristic roots of a 2-DOF SISO system as μ_c increases from 0 to 1 are shown in Figure 9a (for the system with an ideal actuator) and Figure 9b (for the system including the actuator dynamics). It can be seen that within this range both systems are always stable, provided they are properly tuned.

Figure 9 also shows the root locus diagram when the absorber damping and mass are fixed, and the absorber stiffness varies from zero to infinity. Unlike the VSD controller, the pattern of alternating poles and zeros is preserved despite the inclusion of the actuator dynamics. This behaviour can also be observed when the root locus is plotted for changing absorber damping rate, or when the absorber mass ratio is modified. However, if the proof-mass dynamics are included then the system can possess zeros and/or poles which lie to the right of the imaginary axis. This indicates that if the absorber becomes sufficiently de-tuned, then instability can still occur.

In summary, the VPA control strategy is not destabilised by the dynamics of the proof-mass provided the virtual absorber is reasonably well tuned. In this study, the controller gain was chosen to be μ_c=0.05 or μ_c=0.5.

For the virtual passive-active absorber, the optimum gains can also be chosen from Table 1. Since ζ_a and ω_a depend on the value of g_u and μ_c, the classical root locus method is once again inapplicable. To verify stability of the system, loci of characteristic roots of equation (33) are plotted in Figure 10, as g_u increases and $\mu_c = 0.05$. In this case, the proof mass dynamics did not strongly affect the stability of the system. However, the number of structural modes that were modelled had a critical effect. This is illustrated in Figure 10, where the model of the structure is either 1DOF (Figure 10(a)) or 2DOF (Figure 10(b)). If the structure model includes only the first mode of vibration (as shown in Figure 10(a)), then the system is stable until $g_u < 1$. In contrast, the 2DOF structure (Figure 10(b)) can become unstable due to the locus corresponding to the second mode of vibration. This indicates that stability and performance of the VPAA controller is influenced by the higher mode dynamics of the system. It should be noted that the stability condition suggested by Nishimura *et al* (1998,

equation (2)) therefore only applies to single-degree-of-freedom structures. To ensure stability of the control system, the value of $g_u = 0.1$ and $\mu_c = 0.05$ were selected in this study.

Now that the stability of the control strategies has been explored, and controller gains have been chosen, the experimental performance can be compared to simulated behaviour.

Results

To illustrate the performance of the various control systems, the open and closed loop behaviour will be compared using both experimental and simulated frequency response functions. The experimental closed loop FRF's were obtained using the hardware previously described and illustrated in Figure 4. The corresponding simulations were performed based the modelled transfer functions of the structure and actuator, combined with the analytical control laws to predict the system's frequency response.

Figure 11(a) presents the results for the virtual skyhook damping controller, and compares them to the open loop behaviour. The damping of the first mode of the structure was increased from 0.002 to 0.075 using virtual skyhook damping, resulting in a 30 dB reduction in peak vibration magnitude. The model accurately predicts the experimentally observed behaviour, for the first two modes.

In Figure 11(b) this result is repeated for the virtual passive absorber control with Den Hartog tuning for the first mode of vibration, and a mass ratio of 0.05. As expected the resonant peak is replace by two nearly equal peaks of lower magnitude. Compared to the VSD controller, a similar performance is observed for the first mode of the vibration, but the vibration of the higher frequency modes of the structure is worse. The model again accurately predicts the observed behaviour of the first two modes. The corresponding result for a Juang-optimised VPA (Table 1) was nearly identical to Den-Hartog's method (despite the difference in damping ratio of the absorber) and so is not included here.

The VPA controller can be extended to control more than one mode of vibration, with a passive analogy of using more than one vibration absorber, each being tuned to a different frequency. Figure 11(c) illustrates the behaviour when this control strategy is used to control the first two modes of vibration. In this case the VPA mass ratios were set to 0.5 for the first mode and 0.05 for the second mode, and the proof-mass actuator was situated at position X_3 in order to control the second mode of vibration.

The results from the virtual passive/active vibration absorber are illustrated in Figure 11(d). Upon direct implementation, the controller exhibited a high level of sensitivity to measurement noise, and so a second-order low-pass filter was implemented as the compensator shown in Figure 7. Even with this, the experimental response is still considered rather poor and noisy, especially at higher frequencies. Despite the good damping performance for the first mode of vibration, the lack of control smoothness and additional order of the controller due to the low-pass filter makes this control strategy less attractive in practice.

For all the experimental results the corresponding model has accurately predicted the behaviour, which validates the modelling approach. In Figure 12 the validated model is used to illustrate the control energy required for each controller configuration. Here, the FRF of the control voltage to disturbance force is plotted. Virtual skyhook damping exhibits a relatively broadband FRF, since it is not a mode-specific control strategy. In contrast, the virtual passive absorber tuned to a single frequency focuses its control effort in a narrow frequency range.

Discussion

It is clear that all of the control strategies have been effective in attenuating the vibrations of the workpiece. Although the background theory of machine tool chatter is beyond the scope of this paper, it is relatively straightforward to demonstrate that increasing the structural

damping will have increased the chatter stability of the workpiece. The purpose of this penultimate section is to critically compare the controller performance and to consider which strategy is most appropriate in practical machining problems.

First, it is worth pointing out that this study has specifically considered the role of the low frequency dynamics of the proof-mass actuator. Although it has been shown how this can de-stabilise the control strategies, other factors could also potentially lead to system instability. For example, if the natural frequencies of the structural modes approach the bandwidth of the actuator or sensor, then the pattern of alternating poles and zeros will be disrupted, so stability is no longer guaranteed. A similar problem would arise if the sensor and actuator were not properly co-located.

The experimental responses of the structure with the virtual passive-active absorber controller were very sensitive to measurement noise, thus resulting in poor structural responses. Since the control effort of the controller is not attenuated at high frequency range, all undesirable high frequency signals will therefore be amplified and fed through the structure. To remedy the problem, a low-pass filter was included to the controller in this study. However, the resulting structural responses were still poor compared to the other controllers. Consequently, the virtual passive absorber controller with a high value of mass ratio is considered more appropriate.

Theoretically, the virtual skyhook damping with an acceleration feedback appears to be the easiest to implement since only one control parameter (the gain) need be chosen. However, the controller is impractical to directly implement since a DC-offset signal associated with the accelerometer was built up as a result of the integral controller. A second-order high pass filter was included to the controller in this study to eliminate the DC-offset built-up. Moreover, it has been shown here that the actuator dynamics can cause instability, so some formal control design procedures (e.g. root locus) are required. In Chung's work (1997), this

instability had to be overcome by including a compensator in the control strategy. In contrast, the virtual vibration absorber can be tuned using simple formulae, and for the problem considered here, the tuned control strategy was always stable.

It can be shown (eg Delio et al. (1992)) that chatter is caused by one mode of vibration of the structure, and its corresponding natural frequency will contribute to the chatter frequency. This suggests that the control effort can be focused on the problematic mode of the structure using a mode-specific controller such as the virtual passive absorber. Moreover, chatter is not the only vibration occurring during milling, since there are forced vibrations arising from rotation of the cutting tool into the workpiece. Since skyhook control energises the structure across the whole frequency range (Figure 12), significant control energy is consumed by damping the forced vibration of the structure. This will have no contribution to increasing the chatter stability, and is more likely to cause saturation of the actuator.

It is clear that the virtual absorber strategy can be an alternative solution to the skyhook strategy in mitigating chatter. However, to accurately tune the controller at the problematic mode of vibration may require knowledge of the structure's frequency response, along with an indication (from chatter theory) of which mode will be 'problematic'. In this case, it transpires that this information can be gleaned from audio signals during machining (Delio et al. (1992)), which paves the way for a further development of adaptive control based upon the virtual passive vibration absorber strategy. A further complication is the robustness of the strategy to changes in the dynamics of the host structure. For the problem of a workpiece during milling, the dynamics will change as material is removed during machining. For some machining operations such as finishing cuts, the volume of material removed may be so small that the absorber does not need to be retuned. However, if the workpiece dynamics change considerably then the controller gains may need to be time-varying, or adaptively retuned.

A final issue worth discussing is how the virtual passive absorber compares to its physical counterpart. A simple passive vibration absorber would of course require no control circuitry and no source of power. However, such a device often has fixed properties for mass, stiffness, and damping. Even if some rudimentary tuning is possible, this must be done by hand rather than automatically. Consequently the device is of limited use if the dynamics of the vibrating structure are likely to change. Furthermore, the passive device must typically weigh at least 5-10% of the effective mass of the problematic mode of vibration. This cannot always be achieved in practice due to the load restrictions of the machine. With an active approach the virtual passive controller can achieve the same performance but only the mass of the actuator need be considered – the remaining hardware can be remotely located. For example, in the present study the actuator weighed 0.12kg but via the control strategy it behaved as a virtual mass of 0.3kg.

Conclusions

Three controllers, virtual skyhook control, virtual passive absorber control and virtual passive-active absorber control strategy have been demonstrated and evaluated. The low frequency dynamics of a proof mass actuator have been considered in evaluating the controller performance, with particular emphasis on the application of chatter mitigation in cutting processes.

The ‘virtual passive-active absorber’ controller can provide good damping levels, but it is less appropriate due its high sensitivity to measurement noise. The ‘virtual skyhook’ controller is theoretically straightforward to implement, but a high pass filter must be included in practice. The achievable damping rate of the controller is also limited by the actuator dynamics, which can make it necessary to include an additional compensator to the controller and to apply root locus design techniques for each setup.

Alternatively, virtual passive absorbers offer a superior performance provided that they can be tuned to the problematic mode of vibration. Compared to the virtual skyhook controller, the actuator dynamics are less likely to affect stability, and control effort is focussed on the problematic mode of vibration. Consequently saturation due to the forced vibrations of the structure is less likely compared to the virtual skyhook control strategy. For machining problems, the energy supply and drive electronics can be remotely located, so there is a higher performance with a lower weight than for the corresponding passive vibration absorber. However, for machining applications the controller performance will degrade if the structural dynamics change significantly during the cutting process. Possible applications which avoid this problem are the control of workpiece vibrations during finishing operations, or the control of the machine tool structure.

Acknowledgments

The authors are grateful for the support of the Advanced Manufacturing Research Centre with Boeing, at the University of Sheffield. NDS is funded by the EPSRC by an Advanced Research Fellowship (GRS49841/01). SH's PhD studentship is sponsored by Mahanakorn University of Technology.

Optimization method	Natural frequency	Damping ratio
VPA controller (Den Hartog (1985; Ormondroyd and Den Hartog (1928))	$\frac{\omega_a}{\omega_n} = \frac{1}{1+\mu_c}$	$\zeta_a = \sqrt{\frac{3\mu_c}{8(1+\mu_c)}}$
VPA controller (Juang and Phan (1992; Juang and Phan (2001))	$\frac{\omega_a}{\omega_n} = \frac{1}{1+\mu_c}$	$\zeta_c = \sqrt{\frac{\mu_c}{4(1+\mu_c)}}$
VPAA controller (Nishimura et al. (1992))	$\frac{\omega_c}{\omega_n} = \frac{\sqrt{1-g_u}}{1+\mu_c}$	$\zeta_c = \sqrt{\frac{3(\mu_c+g_u)}{8(1+\mu_c)}}$

Table 1: Optimum passive absorber parameters

Mode	Natural Frequency ω_i	Damping ratio ζ_i	Modal constant, ψ_{ij}^2		
			X_1	X_2	X_3
1st	432.5Hz	0.0018	1.3240	1.3240	1.3240
2nd	1150Hz	0.012	0.6459	0.00	-0.6459
3rd	1627Hz	0.0011	0.0292	0.0292	0.0292
4th	1701Hz	0.0004	0.0018	0.00	0.0018

Table 2: Modal parameters of the test structure

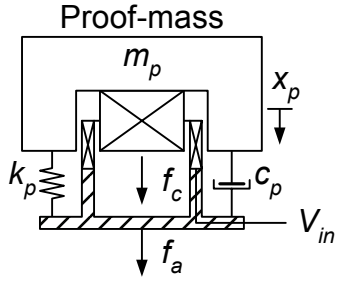

Figure 1: Proof mass actuator

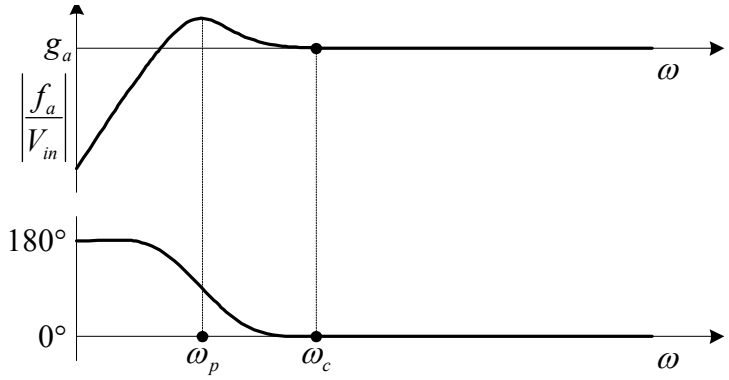

Figure 2: Bode plot of an idea proof-mass actuator

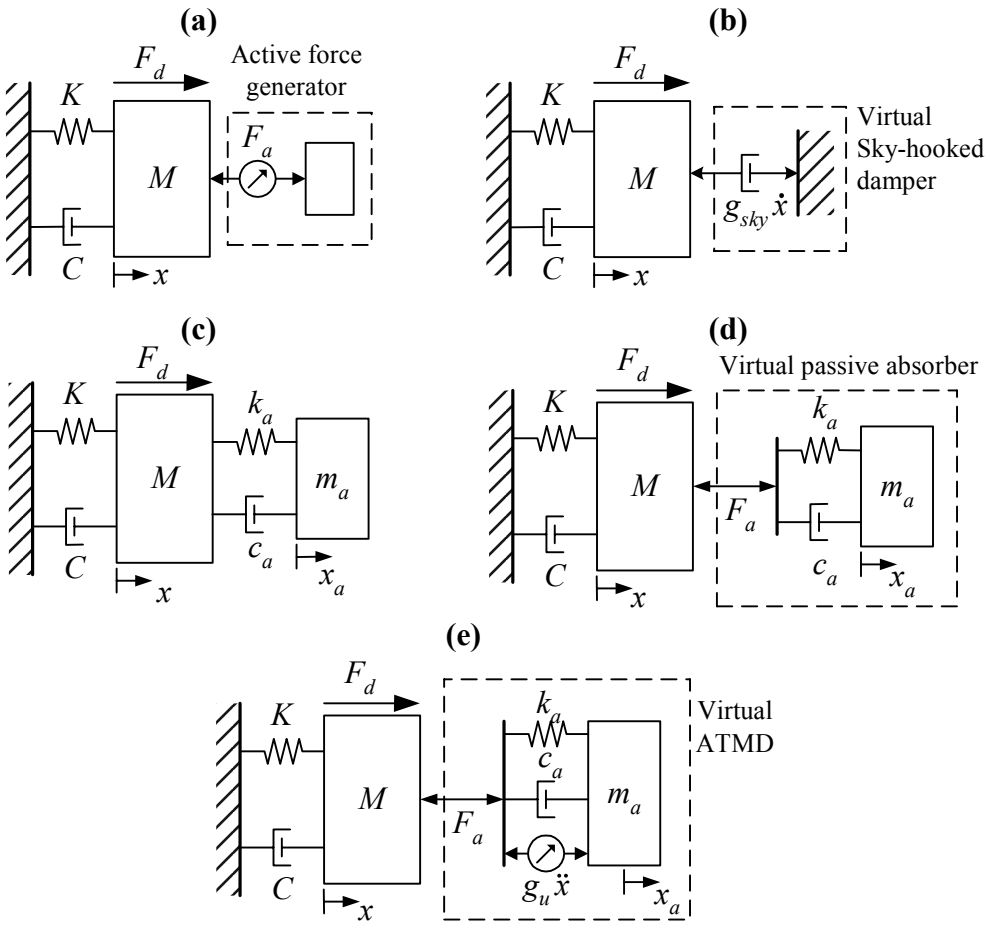

Figure 3: Schematic representation of the control laws. (a) Proof mass actuator performing active vibration control (b) Virtual skyhook damper (c) Passive vibration absorber (d) Virtual passive absorber (e) Virtual active tuned mass damper, or virtual passive/active absorber

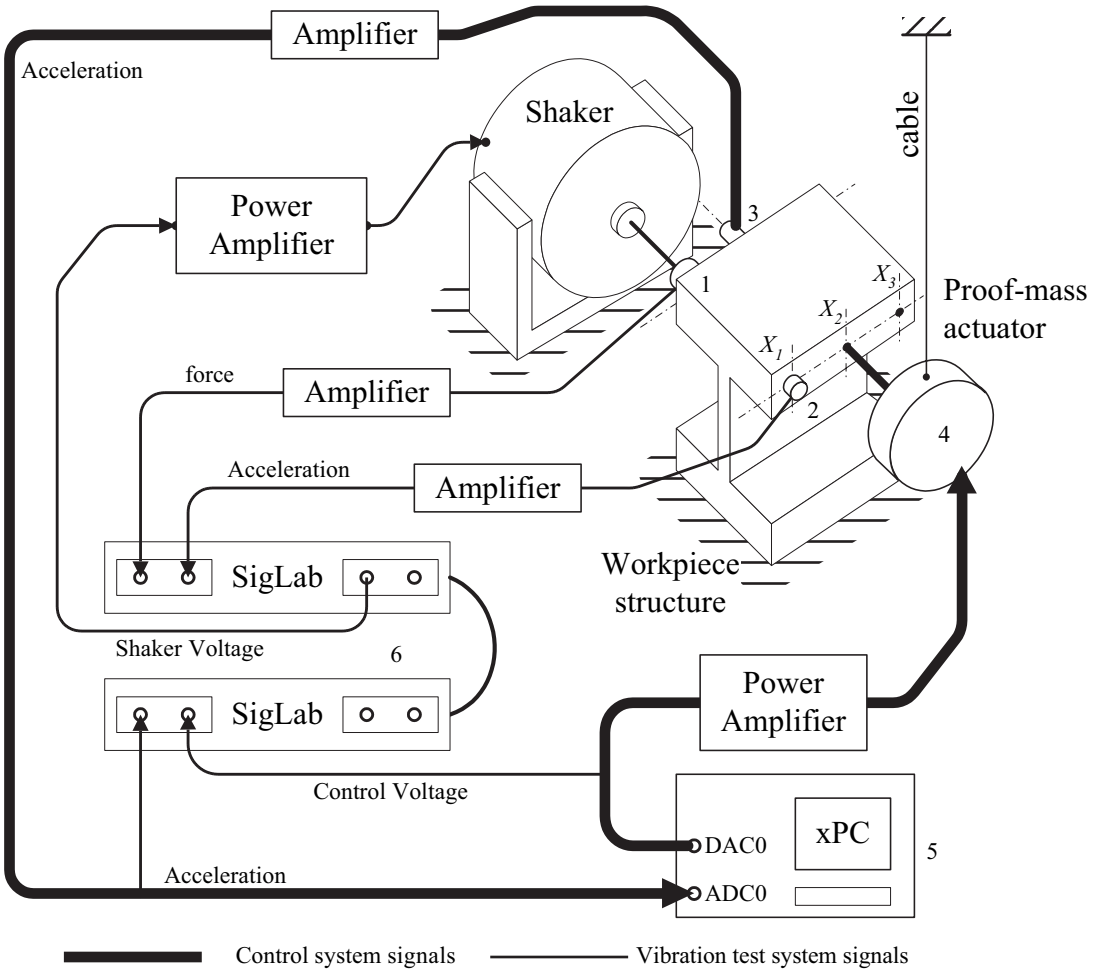

Figure 4: Active control system arrangements

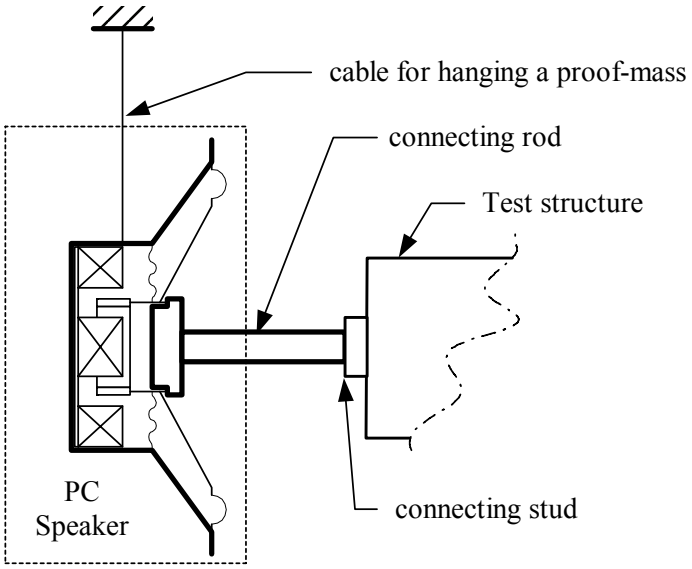

Figure 5: PC-Speaker as a proof-mass actuator

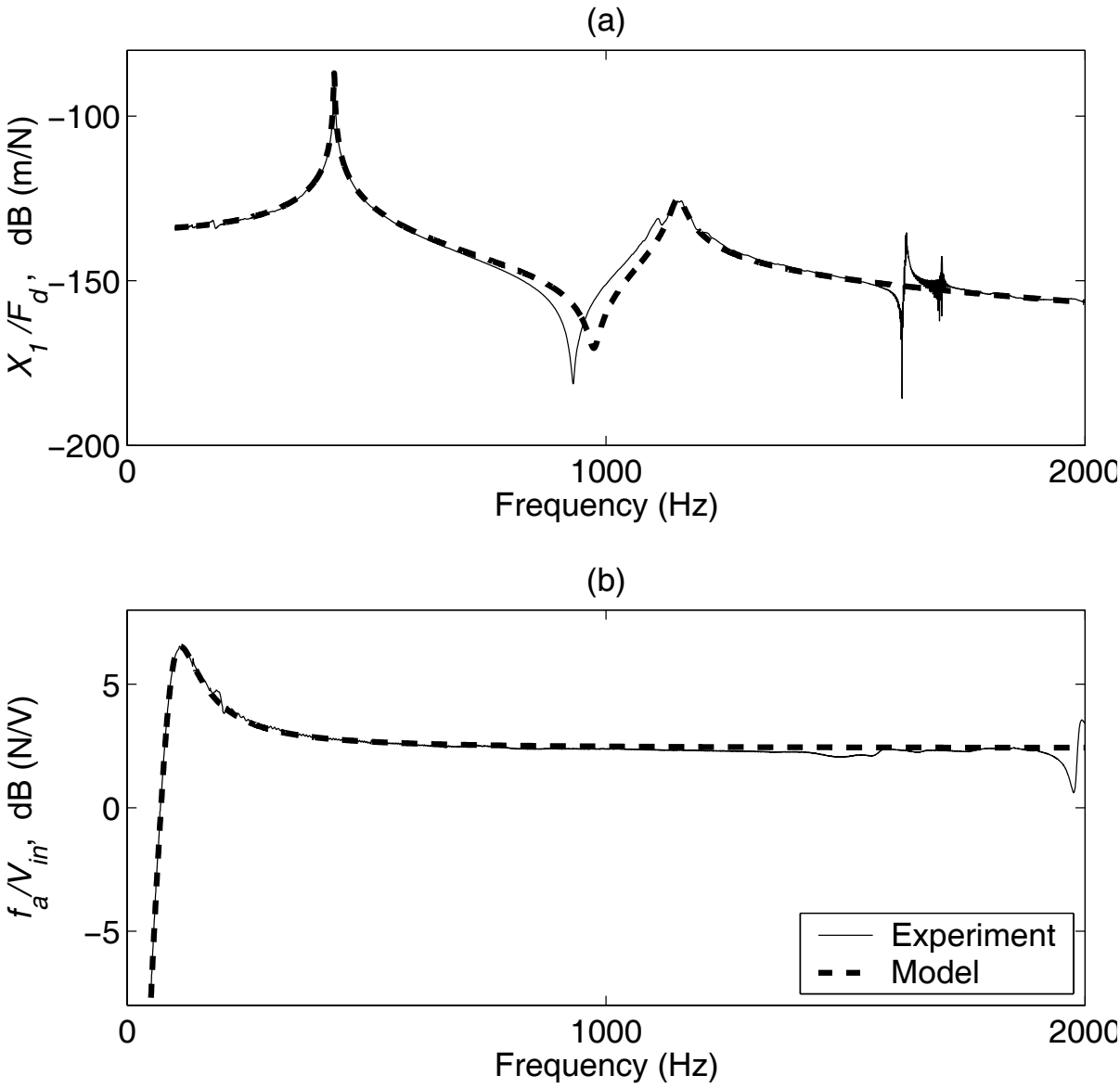

Figure 6: Experimental and modelled frequency response functions.
(a) Workpiece structure (b) Proof-mass actuator.

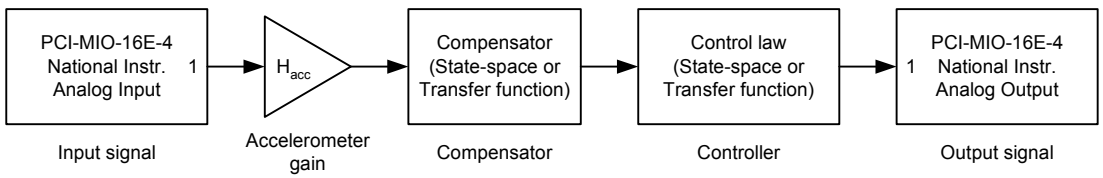

Figure 7: A basic Simulink model of controller

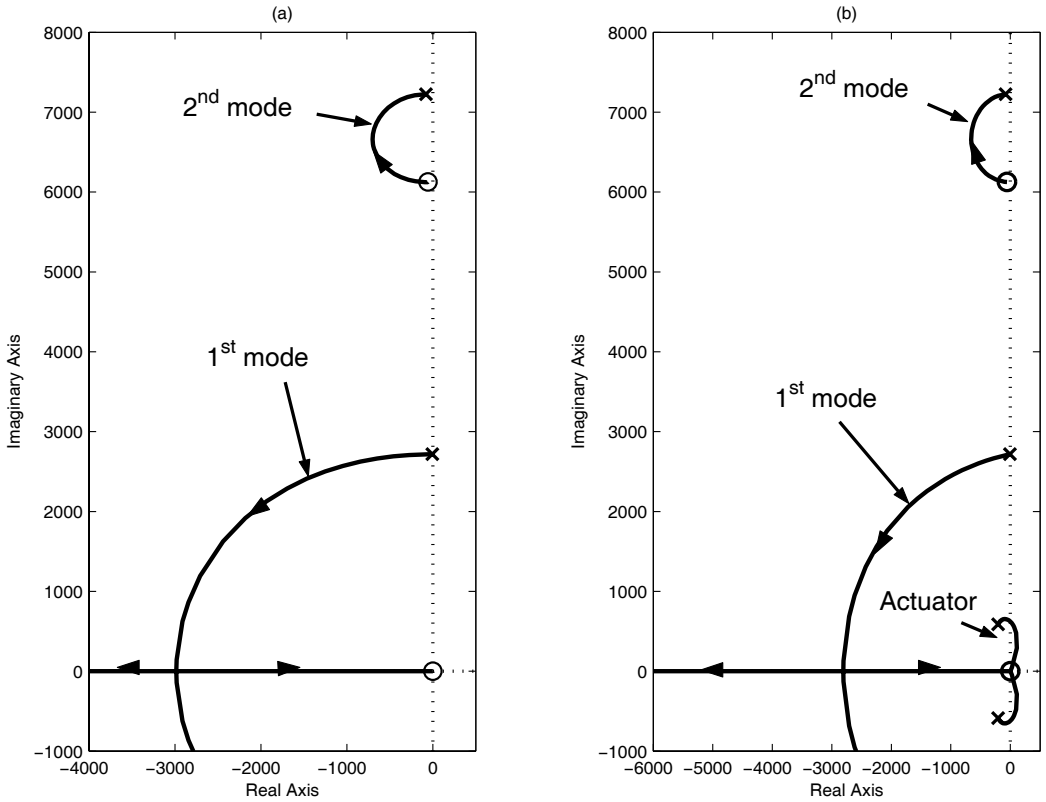

Figure 8: Root-locus plot of the structure with virtual skyhook damping.
(a) without actuator dynamics (b) with actuator dynamics

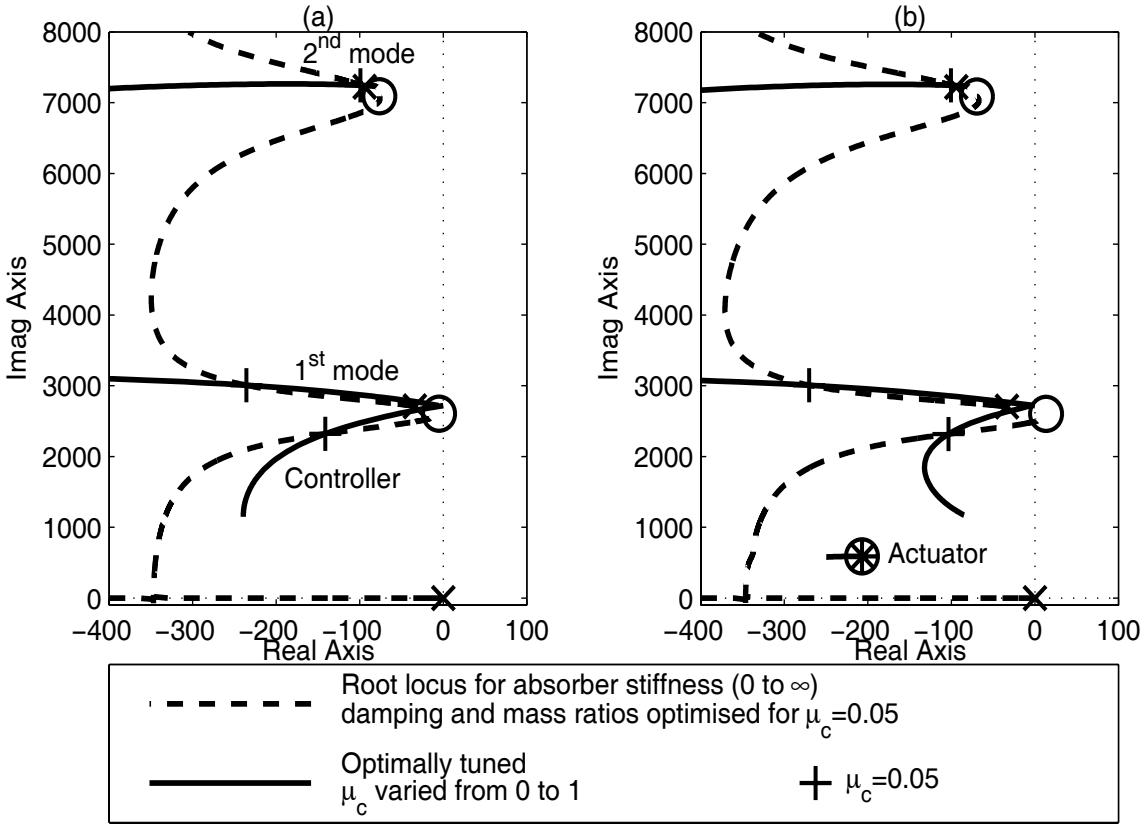

Figure 9: Loci of characteristic roots of the structure with virtual passive absorber controller.
(a) without actuator dynamics (b) with actuator dynamics

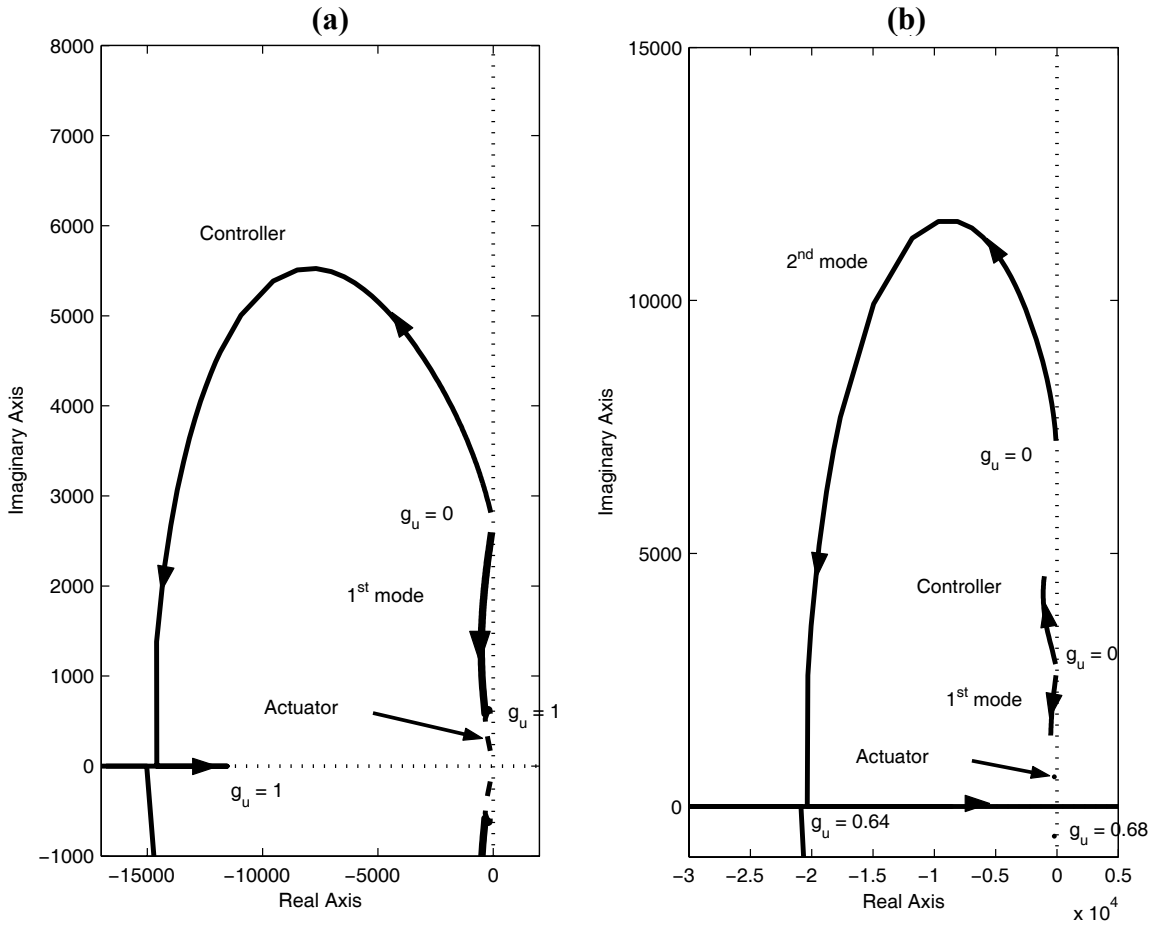

Figure 10: Loci of characteristic roots of the structure with virtual passive/active absorber controller with actuator dynamics. (a) 1DOF structural model (b) 2DOF structural model

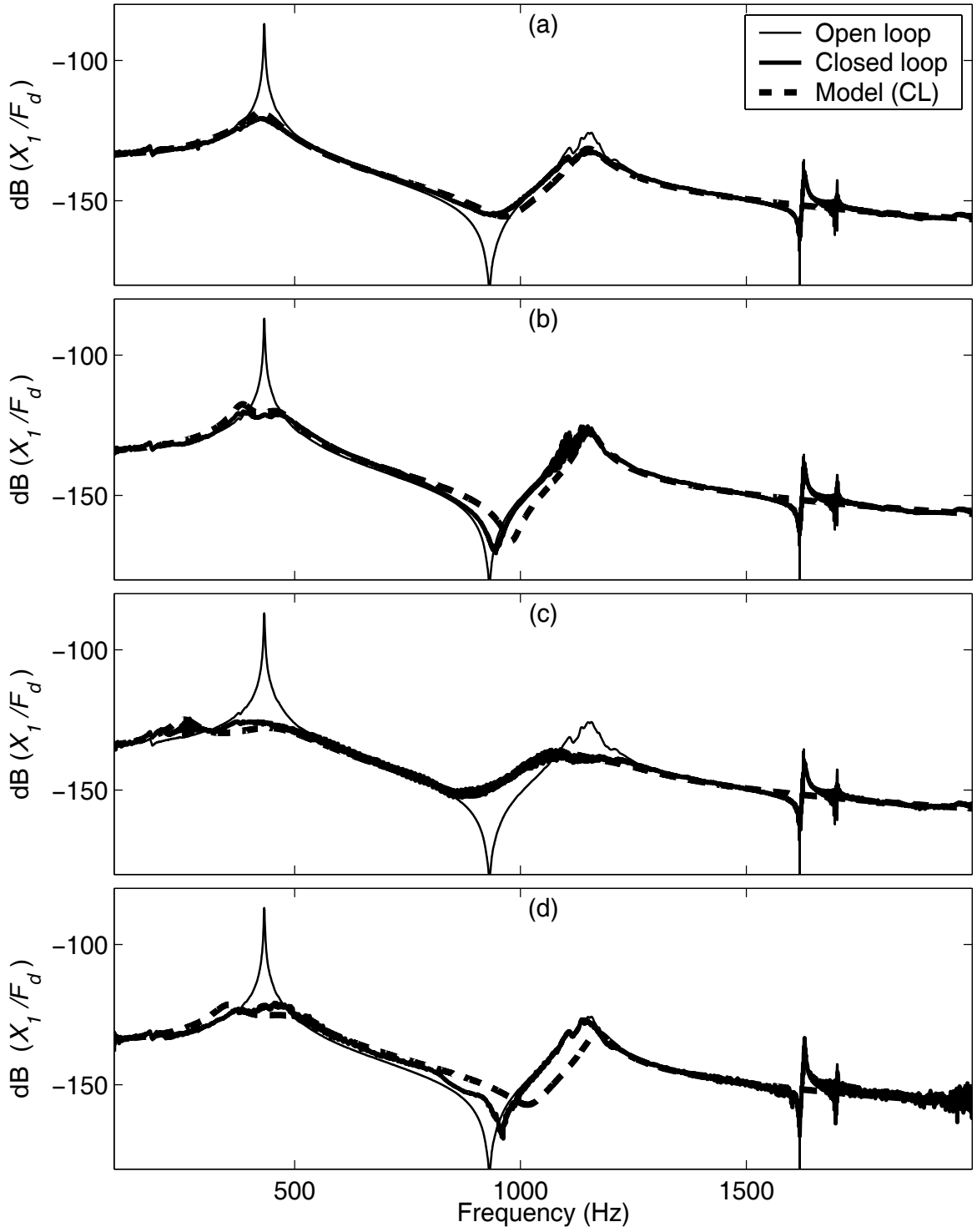

Figure 11: Simulated and experimental frequency response functions.
(a) Virtual skyhook damping at X_2
(b) Virtual passive absorber at X_2. Den Hartog optimisation, μ_c=0.05.
(c) Multi-mode virtual passive absorber at X_3. μ_c=0.5 (mode 1) and μ_c=0.05 (mode 2).
(d) Virtual passive-active absorber at X_2.

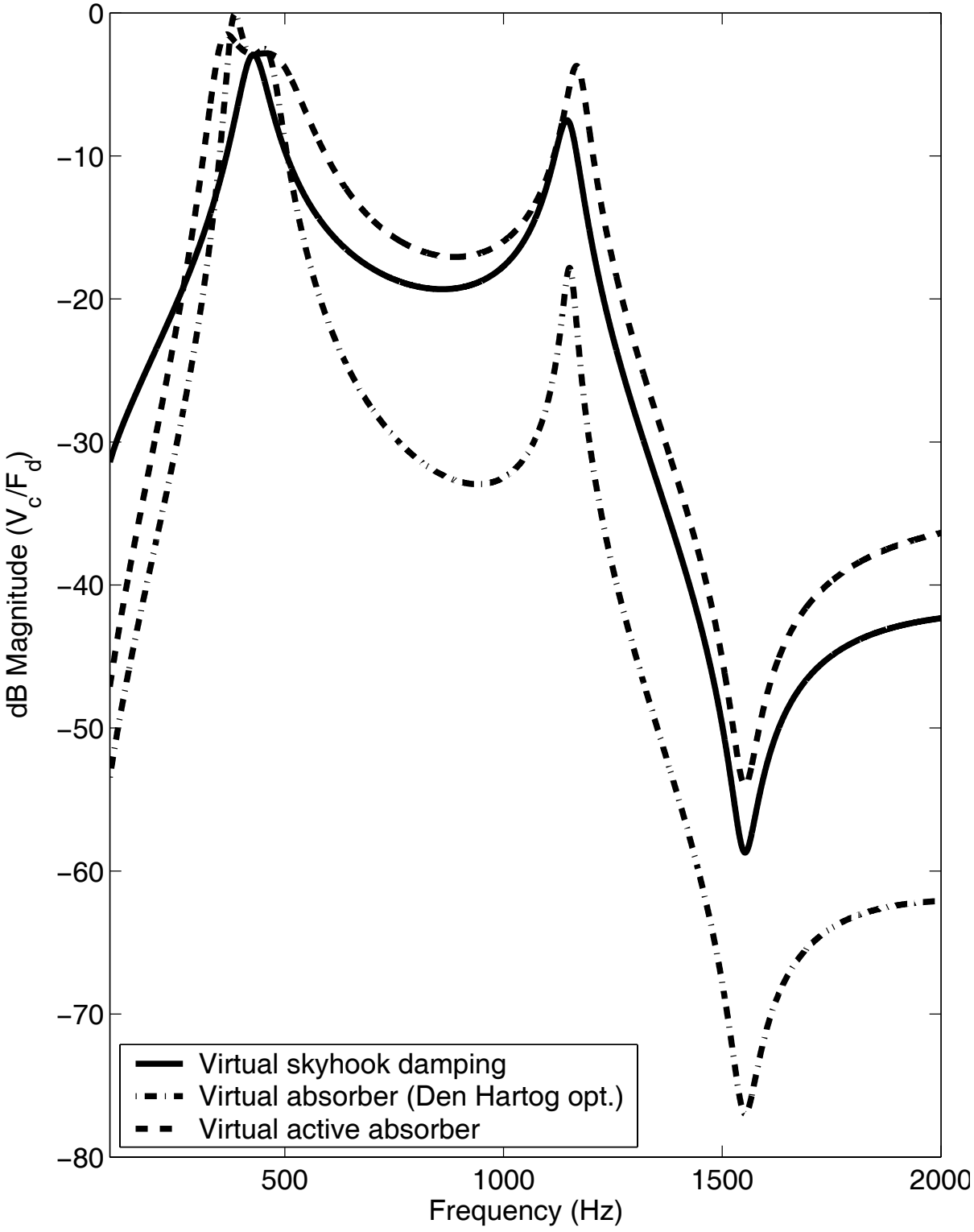

Figure 12: FRF of the control voltage as a function of disturbance force.

References

Cao, T.-T. V., Chen, L., He, F., and Sammut, K. 2000. "Adaptive Integral Sliding Mode Control for Active Vibration Absorber Design." *Conference on Decision and Control*, Sydney, Australia.

Chung, B., Smith, S., and Tlusty, J. 1997. "Active Damping of Structural Modes in High Speed Machine Tools." *Journal of Vibration and Control*, **3(3)**, 279-295.

Delio, T., Tlusty, J., and Smith, S. 1992. "Use of Audio Signals for Chatter Detection and Control." *Journal of Engineering for Industry*, **114**, 146-157.

Den Hartog, J. P. 1985. *Mechanical Vibrations*, Dover, New York.

Ewins, D. J. 2000. *Modal Testing: Theory, Practice, and Application*, Research Studies Press.

Ganguli, A., Deraemaeker, A., Horodinca, M., and Preumont, A. 2005. "Active damping of chatter in machine tools - demonstration with a 'hardware-in-the-loop' simulator." *Journal of Systems & Control Engineering*, **15**, 359-369.

Guclu, R., and Sertbas, A. 2005. "Evaluation of sliding mode and PID controlled structures with an active mass damper." *Journal of Vibration and Control*, **11**, 397-406.

Hagood, N. W., and Crawley, E. F. 1991. "Experimental investigation of passive enhancement of damping for space structures." *AIAA Journal of Guidance*, **14(6)**, 1100-1109.

Juang, J.-N., and Phan, M. 1992. "Robust controller designs for second order dynamics systems, a virtual passive approach." *Journal of Guidance, Control and Dynamics*, **15(5)**, 1192-1198.

Juang, J.-N., and Phan, M. 2001. *Identification and Control of Mechanical Systems*, Cambridge University Press, Cambridge.

Nishimura, I., Kobori, T., Sakamoto, M., Koshika, N., Sasaki, K., and Ohrui, S. 1992. "Active tuned mass damper." *Smart Materials and Structures*, **1(4)**, 306-311.

Nishimura, I., Yamada, T., Sakamoto, M., and Kobori, T. 1998. "Control performance of active-passive composite tuned mass damper." *Smart Materials and Structures*, **7(5)**, 637-653.

Ormondroyd, J., and Den Hartog, J. P. 1928. "The Theory of the Dynamic Vibration Absorber." *Journal of Applied Mechanics*, **50**, A9-A22.

Pratt, J. R., and Nayfeh, A. H. 2001. "Chatter control and stability analysis of a cantilever boring bar under regenerative cutting conditions." *Philosophical Transactions of the Royal Society of London, Part A*, **359**, 759-792.

Preumont, A. 2002. *Vibration Control of Active Structures, An Introduction*, Kluwer Academic Publishers, Netherlands.

Tlusty, J. 2000. *Manufacturing process and equipment*, Prentice-Hall.

Wang, Y. Z., and Cheng, S. H. 1989. "The Optimal Design of Dynamic Absorber in the Time Domain and the Frequency Domain." *Applied Acoustics*, **28**, 67-78.